Composites Science and Technology 71 (2011) 350–356

Contents lists available at ScienceDirect

Composites Science and Technology

journal homepage: www.elsevier.com/locate/compscitech

Effect of porosity on the interface behavior of an Al_2O_3–aluminum composite: A molecular dynamics study

Chinmaya R. Dandekar, Yung C. Shin *

Center for Laser-based Manufacturing, School of Mechanical Engineering, Purdue University, West Lafayette, IN, United States

ARTICLE INFO

Article history:
Received 4 May 2010
Received in revised form 15 November 2010
Accepted 30 November 2010
Available online 4 December 2010

Keywords:
A. Metal matrix composites
B. Weibull model
C. Computational modeling
Molecular dynamics

ABSTRACT

Molecular dynamics simulations are carried out to study the effect of porosity and temperature on a ductile–brittle interface under tensile and shear loadings. Traditionally the interface is characterized by a cohesive zone model (CZM) with the traction–separation law assumed or parameterized through experiments, where the experimental determination of the shape of the CZM has proven to be difficult. In this study a traction–separation law is thus obtained for an alumina–aluminum composite system by conducting molecular dynamics simulations. A statistical approach is suggested to characterize the cohesive strength in the parameterized traction–separation law via the Weibull distribution, which consequently governs the interface behavior of the composite.

1. Introduction

Metal matrix composites (MMC) offer high strength to weight ratio, high stiffness and good wear resistance resulting in an ever increasing use in the aerospace, automotive and bio-medical industries. Popular reinforcement materials for these composites are silicon carbide and alumina particles, while aluminum, titanium and magnesium are the most common matrix materials. The mechanism of failure at the microscale is dominated by factors such as the cohesive strength of the interface, and the strength and reliability of the particle and matrix phase. The interface between the reinforcement and matrix plays a crucial role in changing the property of composite material. In many cases the properties of MMC can be drastically altered by the nature of the interface, making it necessary to understand the characteristics of the interface [1]. However, experimental difficulties in studying interface failure and limitations in analytical methods due to complex interfacial reactions have hampered the development of models capable of predicting the interfacial quantities. Contemporary materials design therefore seeks to improve material performance by understanding material behavior at the nanometer level and thereby predicting the mechanical properties of the interface.

A number of different approaches have been considered for modeling the interface, among which the cohesive zone models are widely used to model delamination and debonding in composite materials [2–4]. A limitation of traditional continuum mechanics models is the inability to imbide the variation in the size and attributes of the microstructure. However, this limitation can be overcome by utilizing a Weibull distribution to characterize the cohesive strength of the interface.

Cohesive zone models (CZM) are known to imbibe idealized traction–separation behavior for modeling interface debonding, transgranular and intergranular fracture. Traditionally the cohesive zone laws have been assumed rather than being predicted, or are parameterized through empirical data, obtained by using the macroscopic fracture toughness of the material [3] or by conducting nanocrystalline experiments to obtain the traction–separation data [5]. The problem with using macroscopic/empirical values of fracture toughness is that these are aggregate responses of hundreds of thousands of grains applied to local interfaces where the fracture/debonding occurs. This problem is addressed by conducting MD simulations on the interface between the particulate and matrix to obtain a traction–separation relationship.

A number of groups have attempted to extract relevant parameters for a traction–separation law for the CZM from atomistic (MD) simulations [6–11]. Some of these approaches have been limited to studying the deformation of single phase materials. Komanduri et al. [6] carried out uniaxial tensile tests, while Spearot et al. [7] simulated crystal deformation under both tensile and shear loads on systems on the order of 4–8 nm (too small when compared to CZM models in continuum simulations). The small system size and the applied boundary conditions resulted in the suppression of plastic deformation processes, such as slip dislocation. Yamakov et al. [8] improved these earlier attempts by expanding the simulation domain to simulate intergranular fracture in a bi-crystal of aluminum under tensile loading (Mode

* Corresponding author.
E-mail address: shin@purdue.edu (Y.C. Shin).

0266-3538/$ - see front matter © 2010 Elsevier Ltd. All rights reserved.
doi:10.1016/j.compscitech.2010.11.029

I). Gall et al. [9] modeled the interface behavior between two dissimilar materials, aluminum (Al) and silicon (Si) under tensile loading to demonstrate the ability of a modified embedded atom method (MEAM) potential model. Zhou et al. [10,11] simulated fracture between two B.C.C type brittle materials under combined tensile loadings to arrive at traction–separation laws.

Composite materials demonstrate varying strength due to the presence of dislocation, vacancy defects, porosity and chemical impurities. To address this issue, Gall et al. [9] conducted a limited study using MD on the effect of vacancy defects on the stress–strain response of an Al–Si interface. The authors concluded that increasing point vacancy defects resulted in the lowering of the overall cohesive strength. Although the study was limited, in terms of system size, mode of loading and temperatures, it demonstrated the important observation on the interface strength in the presence of such defects. A popular solution in characterizing the variation in the composite strength is through statistical modeling. The Weibull distribution has been extensively used for many years to determine the static and dynamic failure of numerous materials including alumina–aluminum composites [12,13].

The present study considers the deformation of the interface between pure FCC aluminum and alumina in the presence of porosities. Mode I and Mode II traction–separation relationships for a oxide–metal system (Al_2O_3–aluminum MMC) are also established as a function of temperature. The failure of the interface in the presence of porosities is characterized via a Weibull distribution. In this manner the survival probability of the interface is modeled. The results of this study augment the findings of numerous experimental works related to characterization of the interface.

2. Materials and methods

As the dimensions of the material reach sub-micron length scales, the continuum description of materials becomes questionable and hence a need arises to predict failure at the nanoscale by understanding the atomistic behavior of materials [14]. The power provided by molecular dynamics (MD) simulation is the ability to study the very fundamental processes, simply by applying Newton's law to the description of atomic interactions and thus MD has been used in studying numerous phenomena including: dislocations, cracking, grain boundary sliding, friction, adhesion, melting, diffusion, etc.

The MD simulations in this study were conducted using the open source MD program LAMMPS [15]. For visualizing the evolution of the atomic structure, the Visual Molecular Dynamics (VMD) [16] open source software was used. One of the drawbacks of MD is the *a priori* estimate of atomic interactions, i.e., the interactive forces between various atoms. This interaction is generally represented in the form of an interatomic potential energy model, making it imperative to accurately quantify the interatomic potential of the simulated materials.

2.1. Modified embedded atom method (MEAM) potential

Metals and semiconductors cannot be modeled using pairwise forces. Use of pair potentials to model metals requires extreme care, and any ambiguity automatically invalidates the results because the elastic properties of the solids are not accurately represented. Therefore many-body potentials such as the embedded atom method (EAM) potential has been popularly applied in studying the behavior of numerous metals including aluminum. Although the EAM has been successful in studying metals, it lacks the information needed to represent the electronic orbitals in ionic compounds such as alumina and hence fails to accurately represent them. This led to the development of the modified embedded atom method (MEAM), which includes the angular dependencies to describe the electronic orbitals [17,18]. The MEAM potential is conceptually similar to the EAM potential but differs in added bond angle terms. It is thus suitable for modeling metals and alloys with fcc, bcc, hcp and diamond cubic structures, and covalently bonded materials like silicon and carbon as well as ionic compounds such as alumina.

In the MEAM model the total energy is represented by Eq. (1).

$$E_{tot} = \sum_i \left\{ F_i(\bar{\rho}_i) + \frac{1}{2} \sum_{i \neq j} V_{ij}(r_{ij}) \right\} \quad (1)$$

where $V_{ij}(r_{ij})$ is the pair potential as a function of the atomic separation distance r_{ij} between two atoms i and j, F_i is the embedding function, and $(\bar{\rho}_i)$ is the background electron density at site i. Details of the embedding function and subsequent computation of the embedding function and pair energies can be obtained from the literature [17,18].

The MEAM potentials used in this study for Al and O are obtained from Angelo and Baskes [17], while the Al–O interaction is obtained from Baskes [17,18]. The elastic constants calculated by the MEAM potential for Al are C_{11} = 113.9 GPa and C_{12} = 62 GPa [17] while the elastic constants of Al_2O_3 are C_{11} = 359 GPa and C_{12} = 279 GPa [18]. Additional details of the MEAM potential, and its validity and accuracy of the calculated elastic constants of Al [18], Al_2O_3 [18] and Al_2O_3–Al composite [18] can be obtained from literature.

The simulated structure of pure aluminum is a face centered cubic (FCC) structure with a lattice parameter of 4.05 Å. The crystal structure of α-Al_2O_3 is a part of the hexagonal crystal lattice structure family whose nomenclature is the space group R3-c [19]. The lattice parameters for the conventional unit cell of alumina are a = 4.761 Å, b = 4.761 Å, c = 12.993 Å, $\alpha = 90°$, $\beta = 90°$ and $\gamma = 120°$, where a, b and c stand for the sides of the parallelepiped and α, β and γ the angles between the sides.

Additionally validation of the MEAM potential for Al_2O_3 and Al was conducted by comparing the MD simulated melting temperature to the corresponding *ab initio* and experimental data. For Al a melting temperature of 940 ± 30 K was predicted from the MD simulations, while the melting temperature obtained from *ab initio* calculations for bulk Al was 890–912 K, and the experimentally measured value was 933 K [20]. Similarly, the melting temperature of Al_2O_3 obtained from the LAMMPS MD simulations is 2585 ± 50 K. This compares reasonably well to and the experimentally measured melting temperature of 2330 K [21]. Thus the simulated melting temperature of both materials is in reasonable agreement with the experimental value, thereby validating the selected interatomic potential.

3. MD model and simulation procedure

The fracture behavior of the interface in the presence of porosities predicted by the MD model is shown in Fig. 1. The dimensions in the x–y plane are 50 nm × 60 nm with thickness of 16 nm in the z-direction. The x y z coordinate system represents the lattice directions [0 1 0], [1 0 0] and [0 0 1] respectively. In the model periodic boundary conditions were used in the x and z directions, while it was non-periodic in the y direction. The thickness of the system was carefully selected to prevent suppression of any deformation mechanism such as slip, twin, edge and screw dislocation in the aluminum matrix. Additionally, the thickness is much larger than any of the cutoff distances, thereby preventing the interference of atoms with their periodic images.

Initially, both Al and Al_2O_3 are kept in contact along the interface in the x–z plane with a separation distance of 2 Å. The initial

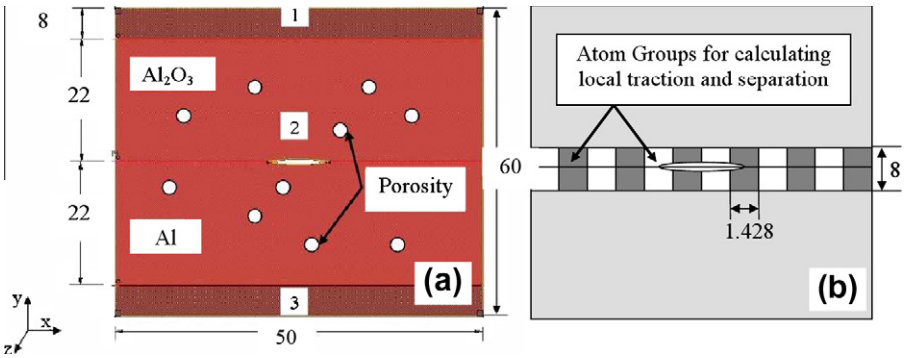

Fig. 1. (a) Simulation of pre-existing crack along the interface, all dimensions are in nm. The crack length simulated is 10 nm and (b) Schematic demonstrating the groups of atoms used in calculating the local tractions and separations.

interface separation distance was chosen close to the equilibrium bond length of Al–Al as the simulated Al_2O_3 crystal is Al terminated. Experimental and theoretical studies suggest that the bulk crystal of Al_2O_3 terminating with a layer of Al yields the most stable structure [22]. The equilibrium bond lengths from *ab initio* calculations and experiments for the Al–O and Al–Al are in the range of 1.79–2.17 Å [23] and 2.49–2.84 Å respectively [24]. Although the initial interface separation distance is not precisely the equilibrium distance, it was shown by Gall et al. [9] that as long as the initial interface separation is not too small or too large to create numerical problems, the separation does not have a large effect on the observed results. Furthermore upon relaxation the interface separation of the Al_2O_3–Al system at room temperature was measured to be in the range of 2.24–2.46 Å. This result is consistent with the equilibrium bond length of Al–Al.

As shown in Fig. 1a, the simulation domain is divided into three regions. Atoms that are in regions 1 and 3 are boundary atoms through which tensile and shear loads are applied. A crack of length 10 nm is generated in the middle of the specimen. During MD simulations of tensile (Mode I) crack propagation, the system is uniformly stretched (by moving each atom a distance corresponding to a uniform normal strain increment) in the *Y*-direction at each time step. Unlike displacing boundary atoms alone, a uniform stretching of the system avoids the creation of shock wave during simulations [11]. During MD simulations of shear (Mode II) crack propagation, the system is uniformly stretched in opposing directions by moving the boundary atoms along the *X*-direction at each time step. Prior to running the simulation, the material state is relaxed for 50 ps to relieve any pre-stress present in the lattice. All the simulations have been carried out at an arbitrarily chosen strain rate of $10^8\ s^{-1}$. A systematic analysis on the effect of strain rate was not conducted in this study. Constant temperature molecular dynamics simulations are carried out at 23 °C, 200 °C, 400 °C, and 600 °C for both the Mode I and Mode II loading for the material lacking in porosity.

3.1. Simulation parameters to study the effect of porosity

To quantify the effect of porosity at room temperature on the interfacial behavior of the Al_2O_3–Al composite the % volume fraction and the size of the pores was adjusted. In this manner the effect of imperfections on the interface strength is accounted for in the composite system. In Al_2O_3–Al composites the porosity is usually present in both phases and the % volume fraction of porosity ranges from 1–10% [1,25,26]. The size of the pores in Al_2O_3 fibers is in the range of nanometers while it can range from a few nanometers to microns in Al. In this study, size of the pores is modeled at the nanometer scale due to the size limitation of MD analysis. Only a limited number of studies have been conducted to study the effect of porosity on the elastic modulus, tensile strength and the fracture strength of the Al_2O_3–Al composite [25,26]. Most of the studies are concerned with the macroscopic behavior of the composite and hence are not suited to represent the interfacial characteristics.

In this study pores are assumed to be present in: (a) only Al (Case A), (b) only Al_2O_3 (Case B) and (c) Al_2O_3–Al (Case C). Pores were randomly distributed in Al and Al_2O_3 for Case A and B respectively. In Case C the coordinates generated for Case A and Case B were used. Table 1 summarizes the parameters selected to study the interface in the presence of porosity.

3.2. System size

Simulations to gage the effect of the simulation domain size on the results were conducted. In this study, following system sizes were selected: $10 \times 15 \times 4$ nm, $20 \times 30 \times 8$ nm, $50 \times 60 \times 16$ nm and $60 \times 70 \times 16$ nm and are referred to as Cases 1, 2, 3 and 4, respectively. This step is important because nanoscale simulations are very sensitive to the size of the simulation box and the number of interacting atoms. Young's modulus of the composite system was observed for systems with varying sizes. The simulations were conducted for Mode I failure at room temperature (300 K). The calculated Young's modulus of Case 1 and Case 2 was 263.16 GPa and 212.62 GPa, respectively. For Case 3 and 4 the simulated Young's modulus was 201.88 GPa and 196.33 GPa, which fell within the Hashin–Shtrikman bounds of 212.78–194.50 GPa calculated from the elastic constants obtained from the MEAM calculations. This validation further instills confidence in the various interatomic potentials selected for this study. Between the system sizes Case 3 and 4 the difference in the Young's modulus is only ~2.7%. Therefore a system size of $50 \times 60 \times 16$ nm offering a good balance in terms of computation time and the required accuracy was selected to conduct the fracture studies. Additionally the stress–strain responses obtained for Case 3 and Case 4 are very similar with a maximum stress of 4.24 GPa and 4.17 GPa and maximum failure strain of 0.138 and 0.143, respectively.

4. Simulation results

4.1. Stress–strain behavior

The overall stress–strain behavior of the composite system was simulated for a perfect interface (no crack present) and a cracked interface in a system with no porosity. The stresses were calculated by using the virial stress theorem [14] for both the tensile and shear stresses. The engineering strain was calculated by comparing the boundary distance from the reference configuration of the

Table 1
Factors and their respective levels in study of the effect of nano-voids on the interface strength in Mode I and Mode II failure.

Factors	Levels		
	1	2	3
Position of nano-void	Aluminum (Case A)	Alumina (Case B)	Aluminum & Alumina (Case C)
% Volume fraction of nano-voids	3	6	9
Nano-void avg. size (radius nm)	3	5	–
Mode of failure	Mode I	Mode II	–

undeformed structure in both the x and y directions. Similar to the methodology outlined by Zhou et al. [10,11], the values of the stresses and corresponding displacements are averaged over 50 time steps to reduce thermal oscillations. Although this averaging is larger than the one outlined in Zhou et al. [10,11], it still allows for a reduction in the thermal oscillations while being computationally efficient.

The simulation results for the Young's modulus, shear modulus and maximum stress are summarized in Table 2. The Young's and shear moduli obtained for the composite system fall within the Hashin–Shtrikman bounds. It can be seen that presence of a crack reduces the maximum load carrying capacity and additionally reduces the stiffness of the composite system.

Further evaluation of the simulation results is made by comparing the maximum stress with analytical results. According to Griffith's theory of fracture, the critical stress (σ_{max}) of fracture for crystalline materials in plane strain can be expressed as shown in Eq. (2). A similar comparison with Girffith's theory in plane stress was done by Zhou et al. [11] for their atomistic simulations on brittle failure.

$$\sigma_{max} = \sqrt{\frac{E \bullet woa}{\pi a_h (1 - \nu^2)}} \tag{2}$$

where E is the elastic modulus of the cracked specimen, *woa* is the work of adhesion, a_h is the crack half length and ν is the Poisson's ratio.

The work of adhesion (*woa*) is defined as the energy required per unit area to reversibly separate the interface into two free surfaces. Theoretically calculated *woa* usually neglects the contribution of plasticity and microstructural defects and usually is less than experimentally characterized *woa*. Streitz and Mintmire [27] developed an MD model to study the adhesion and adhesive failure of an Al_2O_3–Al composite system. The authors concluded that the interface is relatively weak with a maximum failure stress of 2 GPa and a *woa* of 0.3 J/m^2. A drawback of their study is that the simulated system size was very small, i.e., aluminum slab was composed of 48 atoms (12 layers) while the α-Al_2O_3 slab contained 60 atoms (12 oxygen layers). More recently Siegel et al. [22] conducted exhaustive *ab initio* calculations to determine the ideal *woa* and bonding characteristic of the Al_2O_3–Al interface. The authors concluded that for an Al terminated system the *woa* is in the range of 0.41–1.36 J/m^2. The experimental values for the *woa* obtained from literature range from 0.825 J/m^2 to 1.109 J/m^2 [28]. Therefore, by using an average value of 0.933 J/m^2 for the *woa* a maximum stress of 4.26 GPa is predicted, which is close to the simulated value of 4.18 GPa. Thus the results from MD simulations agree quite well with Griffith's theory of fracture. Caution should be exercised in interpreting these results as Griffith's theory of fracture is related to fracture in an isotropic homogenous material. In the study here the equivalent homogenous material properties are utilized in Griffith's failure model. The result presented above is not meant as a validation of the MD simulations but works merely as a spot check of the MD results.

Table 2
Simulation results of Mode I and Mode II failure.

Deformation mode	Crack	Modulus (GPa)	Maximum stress (GPa)
Mode I	No	201.88	4.24
	Yes	186.77	4.18
Mode II	No	78.6	3.20
	Yes	71.43	3.12

4.2. Traction–separation response

MD simulations were conducted for temperatures of 23 °C, 200 °C, 400 °C and 600 °C for Mode I and Mode II failure to develop traction–separation relationships for the CZM. Local tractions and separations were analyzed by following the methodology of Zhou et al. [10,11]. To study the local behavior, the horizontal slot shown in Fig. 1b measuring 8 nm surrounding the crack was further divided into regions (groups of atoms) with width equal to 1.428 nm. A total of 35 regions were obtained and the width of the region allowed for three [1 0 0] planes to be included in each region. The tensile (σ_{yy}) and shear (σ_{xy}) tractions at a local position in the region were calculated as the average atomic stresses (virial) of all atoms in that particular region. As these stresses are calculated locally near the crack surface they therefore relate to the traction in the traction–separation law [9]. Similarly the crack opening displacement (separation) was calculated from the average displacement of the atoms in the region (±40 Å) adjacent to the crack. The opening displacement in normal (Δy) and shear (Δx) therefore are defined and measured as the average atom displacements in the upper half of the region with respect to that of the lower half. Therefore the total magnitude (Δr) of the crack opening is defined as $\Delta r = \sqrt{\Delta x^2 + \Delta y^2}$. Furthermore the stress and crack openings were calculated every 0.2 ps. A study on the effect of measurement location and additional details of calculating the crack opening is available in the literature [9,11].

In general, loading a bi-material interface results in mixed mode crack tip stress intensities, due to the different Poisson's ratios of two materials [29]. It was found that in case of Mode I loading the maximum tensile stress (σ_{yy}) was ~20 times larger than the maximum shear stress (σ_{xy}). Similarly during Mode II loading the maximum shear stress (σ_{xy}) was ~15 times larger than the maximum tensile stress (σ_{yy}). Additionally, the mode-mixity angle or the local loading angle (ψ) was calculated for the MD simulations carried out for Mode I and Mode II loadings. The local loading angle (ψ) is defined as $\psi = \sin^{-1}\left(\sqrt{\frac{\Delta x^2}{\Delta x^2 + \Delta y^2}}\right)$ where Δx and Δy are the shear and normal opening displacements measured within the various groups, which are defined for calculating the local traction–separation curves. The aforementioned definition was successfully applied by Zhou et al. [10,11]. This is consistent with the definition of $\psi = \tan^{-1}\left(\frac{\Delta x}{\Delta y}\right)$, which is used in interfacial mechanics. It is shown that the sin function avoids the "divide-by-zero" problem associated with the tan function during the Mode II loading condition. The final reported value of the phase angle ψ is the average measured phase angle from all the Δx and Δy points obtained from

the MD simulations. The results indicate that the remote and local loading angles are very close to each other. The average phase angle equals ~3.45° and ~85.37° when the remote loading angle is 0° and 90° respectively. The use of remote loads to calculate the fracture mode-mixity is only an approximation for bi-materials with small bi-material constant (0.0332), which is the case in this study. The results give credence to the assumption that the locally obtained traction–separation curves on application of purely Mode I or Mode II remote loadings correspond to either Mode I or Mode II failure dependent on the type of loading. Furthermore complete rupture was not observable during Mode II loading in the system due to the phenomenon of crack healing and sliding of the alumina crystal.

The cohesive model describes a relationship between the interfacial force and the crack opening displacement. In the CZM, the fracture process zone is simplified as being an initially zero-thickness zone, composed of two coinciding cohesive surfaces. Under loading, the two surfaces separate and the traction between them varies in accordance with a specified traction–separation law. In this study the CZM is modeled using Tvergaard's functional form [30] as it represents the MD data reasonably well as shown in Figs. 2 and 3 for Mode I and Mode II loading respectively. Regardless of the temperature of the system or the mode of failure, the traction always initially increases to a peak value and decreases to near zero when the crack opening becomes large. The maximum allowable normal (δ_n = 50 Å) and tangential (δ_t = 75 Å) separation of the cohesive element corresponds to the separation distance at which the traction decreases to near zero value.

The non-dimensional parameter (λ) in Eq. (3) relates the normal (u_n) and tangential (u_t) separation to the maximum allowable normal (δ_n = 50 Å) and tangential (δ_t = 75 Å) separation of the cohesive element. Failure is attained in the cohesive element when the value of λ equals 1. Tvergaard's functional form for the traction–separation law ($F(\lambda)$) is represented as shown in Eq. (4). In Eq. (5) the maximum cohesive strength (σ_{max} = 4.38 GPa) is simulated at room temperature, with the temperature (T) in degrees Celsius. In Eqs. (4) and (5) $\sigma(T)$ is the cohesive strength as a function of temperature. Also obtained from the MD results is the ratio of the shear to normal strength of 0.74, which is necessary in modeling the CZM. Details of the computation of the CZM can be obtained from the literature [30].

$$\lambda = \left\{ \left(\frac{u_n}{\delta_n}\right)^2 + \left(\frac{u_t}{\delta_t}\right)^2 \right\}^{1/2} \tag{3}$$

$$F(\lambda) = \frac{27}{4}\sigma(T)(1 - 2\lambda + \lambda^2) \tag{4}$$

$$\sigma(T) = \sigma_{max}(4.833 - 0.00224\,T - 2.24 \times 10^{-6}T^2) \tag{5}$$

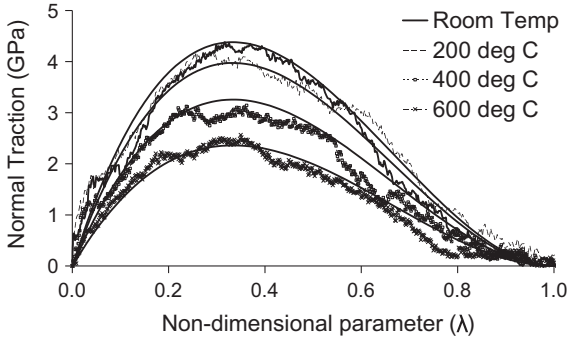

Fig. 2. Traction–separation relationship for Mode I failure in an Al_2O_3–Aluminum Interface. The solid lines represent the parameterized functional form for the CZM.

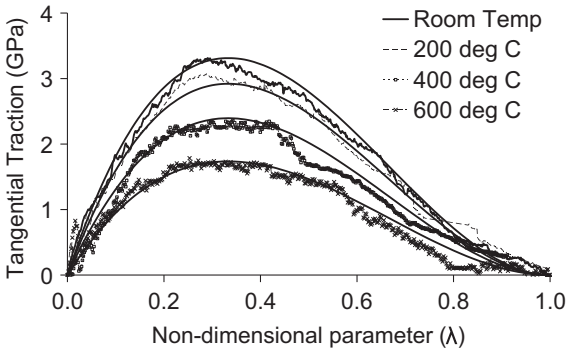

Fig. 3. Traction–separation relationship for Mode II failure in an Al_2O_3–Aluminum Interface. The solid lines represent the parameterized functional form for the CZM.

The work of separation is calculated by integrating Eq. (4) with respect to the separation distance as shown in Eqs. (6) and (7) for Mode I and Mode II respectively. In Mode I and Mode II at room temperature, work of separation is calculated as 12.31 J/m^2 and 13.97 J/m^2 respectively. This shows the work of separation in Mode I is higher than the reported work of adhesion [22,27,28], which is an expected result.

$$G_{IC} = \int_0^{\delta_n} t_n d\delta \tag{6}$$

$$G_{IIC} = \int_0^{\delta_t} t_t d\delta \tag{7}$$

where maximum allowable normal (Mode I) opening is δ_n and maximum allowable tangential (Mode II) opening is δ_t, while the tractions in Mode I and Mode II are represented by t_n and t_t respectively.

4.3. Validation of the CZM

Validation of the MD simulated traction–separation law is done by comparing the simulated work of separation or interfacial fracture energy with experimental measurements of the fracture energy. It should be noted that validation of the MD simulated interfacial fracture energy to experimental results is predominantly qualitative, because experimentally measured interfacial fracture energy is highly dependent on the material yield strength, layer thickness, environmental conditions and interfacial defects. Experimental measurements have shown that the interfacial fracture energy of an Al_2O_3–Al system varies between 15 J/m^2 and 300 J/m^2 and is highly dependent on the thicknesses of the Al layer with respect to the thickness of the Al_2O_3 layer [31–33]. The smallest thickness of the Al layer measured experimentally was 2 μm for

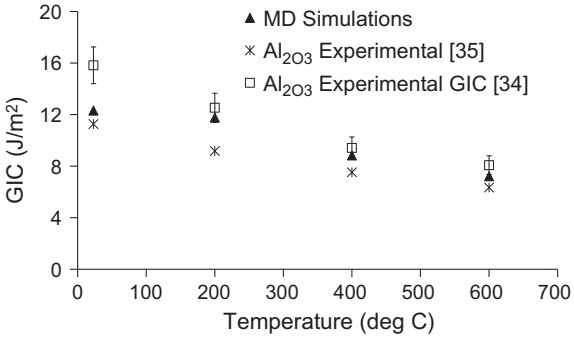

Fig. 4. Fracture energy as a function of temperature for alumina and Al–Al_2O_3 composite.

Table 3
Simulation results for the effect of porosity.

% Volume fraction porosity	Mode I								Mode II	
	Pore radius (3 Å)						Pore radius (5 Å)		Pore radius (3 Å)	
	Case A		Case B		Case C		Case C		Case C	
	Max stress (GPa)	Failure strain	Max stress (GPa)	Failure strain	Max stress (GPa)	Failure strain	Max stress (GPa)	Failure strain	Max stress (GPa)	Failure strain
0	4.43	0.116	4.43	0.116	4.43	0.116	4.43	0.116	3.28	0.228
3	4.34	0.110	4.31	0.120	4.24	0.112	4.24	0.115	3.14	0.223
6	4.25	0.106	4.21	0.126	4.14	0.114	4.16	0.112	3.02	0.224
9	3.90	0.101	4.03	0.130	3.84	0.116	3.88	0.115	2.80	0.225

a corresponding Al_2O_3 layer thickness of 2 μm. At this configuration experimentally measured fracture energy was 15 J/m^2 [33]. On the other hand, the interfacial fracture energy calculated from MD simulations at room temperature is 12.31 J/m^2 for an Al_2O_3–Al sample of equal thickness (22 nm each). The simulated value for the fracture energy with equal layer thicknesses is ~18% lower than the experimental result, which is in reasonable agreement, considering the ambiguity and high degree of variance in the experimental results.

The fracture energy of the interface tends to approach the fracture energy of Al_2O_3 with a decrease in the Al layer thickness [31,32]. Hence, a comparison is made by comparing the MD determined interfacial fracture energy of the composite to the experimentally measured fracture energy of Al_2O_3 [34,35] as shown in Fig. 4. The results indicate a fairly consistent trend of the fracture energy as a function of temperature. To represent a system with reduced Al layer, MD simulations in Mode I at room temperature were carried out on a system with Al layer thickness of 11 nm while keeping the Al_2O_3 layer constant at 22 nm. The interfacial fracture energy of this configuration was measured to be 11.40 J/m^2. An additional simulation was conducted on a pure alumina system at room temperature and the interfacial fracture energy was measured to be 10.83 J/m^2, which is very close to the experimentally measured fracture energy (11.26–15.82 J/m^2) of single crystal Al_2O_3. Care must be taken in the application of MD determined energy release rates as described in the study by Buehler et al. [36].

4.4. Effect of porosity on interface failure

The effect of porosity at room temperature on the interface behavior is analyzed by recording the maximum stress and failure strain of the composite under Mode I and Mode II loading. Table 3 summarizes the simulation results for the maximum stress and failure strain for the cases outlined in Table 1. An expected result in both Mode I and Mode II loading is the reduction in the maximum stress with the increase in % porosity volume fraction for all cases. Additionally, a sensitivity analysis is done to gage the effect of pore size (pores of 3 and 5 nm radius), while keeping the % volume fraction of pores constant for Case C. Mode I simulation results indicate that the maximum stress or the failure strain are not sensitive to the size (radius) of the pores (Table 3) simulated in this study.

The presence of voids also affects the failure strain. In this case, presence of voids in the Al layer (Case A) results in reduced ductility, while the presence of voids in the Al_2O_3 layer (Case B) yields an increase in the ductility as indicated in Table 3. Under Mode II loading the composite failure behavior is similar to the Mode I composite behavior for Case C, wherein the failure to strain remains fairly constant (Table 3).

Fig. 5 compares the trend in the reduction of maximum stress as a function of porosity for Case C between MD simulation results and experimental measurements by Ghosh and Ray [25] for an Al_2O_3–Al composite. Fig. 5 depicts the ratio of maximum stress of the porous material (σ_p) to the maximum stress of the non-porous material (σ_m) versus the % volume porosity. Quite apparent from Fig. 5 is the trend in reduction of maximum stress with an increase in % volume porosity predicted from MD simulations compares very well with experimental measurements.

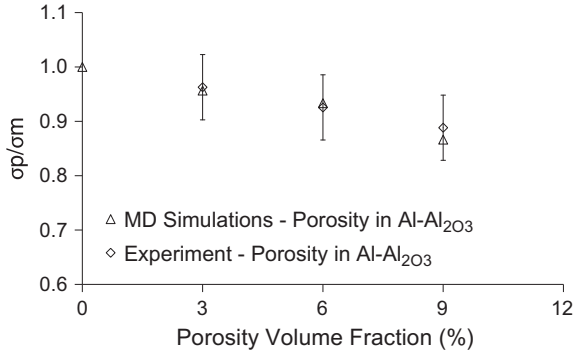

Fig. 5. Effect of porosity on the maximum tensile stress. In the figure σ_p corresponds to the stress related to porous material while σ_m corresponds to the stress related to the non-porous material.

4.5. Weibull model

The Weibull distribution has been extensively used for many years to determine the static and dynamic failure of numerous materials including Al_2O_3–Al composites [12,13]. The survival probability of the interface is modeled via a two-parameter Weibull distribution. In this study a linear regression model is used in the estimation of the two Weibull constants as shown in Eq. (8) for simulation samples with equal dimensions. The survival probability (S) is dependent on the stress (σ), the characteristic

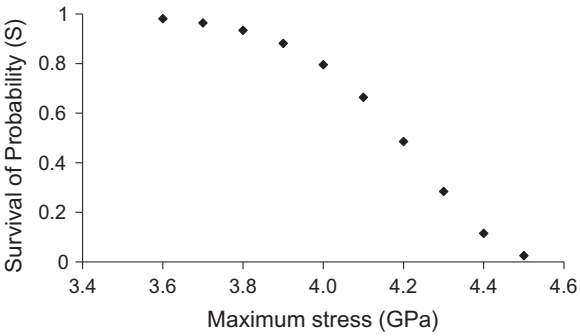

Fig. 6. The survival probability (S) as a function of the maximum interface stress.

stress (σ_o) and the Weibull modulus (m) which is an indicator of the failure rate.

$$\ln\left[\ln\left(\frac{1}{S}\right)\right] = m\ln\sigma - m\ln\sigma_o \tag{8}$$

Additional details on the calculation of the Weibull parameters can be obtained from Babu and Jayabalan [13]. On plotting Eq. (8) using the maximum stress data simulated in Table 3 the Weibull modulus (m) is estimated to be 23.56. Only Mode I data of 0%, 3%, 6% and 9% porosity with pore size of 3 Å is used in calculating the Weibull modulus. The characteristic stress (σ_o) is calculated as 4.25 GPa. The Weibull modulus of an Al_2O_3–Al composite has been experimentally shown to vary from 12.1 to 27.5 dependent on the reinforcement volume fraction [12,13,37]. Lower values of the Weibull modulus are consistent with low reinforcement volume fraction [12,13] while higher Weibull modulus corresponds to a composite with 63% by volume fraction of reinforcement particles. The Weibull modulus obtained from MD studies compares well with experimental results for the Weibull modulus.

Fig. 6 plots the survival probability as a function of the applied stress. This facilitates in gauging the reliability of the composite interface in the presence of applied stress. It is calculated that 36.7% of the simulated specimens have an interfacial fracture strength of at least 4.25 GPa. Additionally the survival probabilities of 0.9 and 0.95 correspond to fracture strengths of 3.87 GPa and 3.75 GPa.

5. Conclusion

MD simulations were carried out to characterize the interface of an Al_2O_3–Al MMC. Traction–separation relationships for Mode I and Mode II failure at high temperatures have been successfully developed through MD simulations. The parameterized traction–separation law based on the MD results is consistent with existing continuum based cohesive zone model. The model predicts the expected result in the reduction of maximum stress with an increase in temperature in both Mode I and Mode II loadings. The simulation results for the interfacial fracture energy compare well with experimental measurements of the same. Increased % volume fraction of porosity resulted in a reduction in the failure stress irrespective whether pores were present in only Al, Al_2O_3 or in both phases. Failure strain on the other hand is dependent on the position of the porosity. Porosity present in only Al resulted in reduced ductility, while porosity present in Al_2O_3 increased the ductility. Pores present in both phases resulted in the failure strain to be fairly constant. A Weibull model was proposed to quantify the effect of porosities on the interface failure stress. The calculated Weibull modulus was 23.56 at a characteristic stress of 4.25 GPa. Simulation results showed good agreement in reproducing the experimentally determined Weibull modulus for an Al_2O_3–Al composite system.

Acknowledgments

The authors wish to gratefully acknowledge the financial support provided for this study by the National Science Foundation (Grant No: 0917936-IIP).

References

[1] Kim J-K, Mai Y-W. Effect of interface strength on MMC properties. In: Kelly A, Zweben C, editors. Comprehensive composite Materials. Pergamon Press; 2000. p. 117–38.
[2] Orifici AC, Herszberg I, Thomson RS. Review of methodologies for composite material modeling incorporating failure. Compos Struct 2008;86:194–210.
[3] Elices M, Guinea GV, Gomez J, Planas J. The cohesive zone model: advantages, limitations and challenges. Eng Fract Mech 2002;69:137–63.
[4] Li S, Thouless MD, Waas AM, Schroeder JA, Zavattieri PD. Use of mode-I cohesive-zone models to describe the fracture of an adhesively-bonded polymer matrix composite. Compos Sci Technol 2005;65(2):281–93.
[5] Wei YJ, Anand L. Grain-boundary sliding and separation in polycrystalline metals: application to nanocrystalline fcc metals. J Mech Phys Solids 2004;52:2587–616.
[6] Komanduri R, Chandrasekaran LM, Raff LM. Molecular dynamics (MD) simulation of uniaxial tension of some single-crystal cubic metals at nanolevel. Int J Mech Sci 2001;43:2237–60.
[7] Spearot DE, Jacob KI, McDowell DL. Non-local separation constitutive laws for interfaces and their relation to nanoscale simulations. Mech Mater 2004;36:825–47.
[8] Yamakov V, Saether E, Phillips DR, Glaessgen EH. Molecular-dynamics simulation-based cohesive zone representation of intergranular fracture processes in aluminum. J Mech Phys Solids 2006;54:1899–928.
[9] Gall K, Hostemeyer MF, Van Schilfgaarde M, Baskes MI. Atomistic simulations on the tensile debonding of an aluminum–silicon interface. J Mech Phys Solids 2000;48:2183–212.
[10] Zhou XW, Zimmerman JA, Reedy ED, Moody NR. Molecular dynamics simulation based cohesive surface representation of mixed mode fracture. Mech Mater 2008;40:832–45.
[11] Zhou XW, Moody NR, Jones RE, Zimmerman JA, Reedy ED. Molecular-dynamics based cohesive zone law for brittle interfacial fracture under mixed loading conditions: effects of elastic constant mismatch. Acta Mater 2009;57:4671–86.
[12] Mussert KM, Janssen M, Bakker A, Van Der Zwaag S. Modelling fracture in an Al_2O_3 particle reinforced AA6061 alloy using Weibull statistics. J Mater Sci 1999;34:4097–104.
[13] Babu AS, Jayabalan V. Weibull probability model for fracture strength of Aluminum (1 1 0 1)–Alumina particle reinforced metal matrix composite. J Mater Sci Technol 2009;25(3):341–3.
[14] Buehler MJ, Gao H. Ultra-large scale simulations of dynamic materials failure. In: Rieth M, Schommers W, editors. Handbook of theoretical and computational nanotechnology, vol. 10. American Scientific Publishers; 2005. p. 1–41.
[15] Plimpton SJ. Fast parallel algorithms for short-range molecular dynamics. J Comput Phys 1995;117:1–19.
[16] Visual molecular dynamics – <http://www.ks.uiuc.edu/research/vmd>.
[17] Angelo JE, Baskes MI. Interfacial studies using the EAM and MEAM. Interface Sci 1996;4:47–63.
[18] Baskes MI. Modified embedded atom method calculations of interfaces. Sandia 1996;96:8484.
[19] NIST structural ceramics database. Standard reference database 2003;30
[20] Vocadlo L, Alfe D. Ab initio melting curve of the fcc phase of aluminum. Phys Rev B 2002;65(21):1–12.
[21] Vashishta P, Kalia RK, Nakano A, Rino J-P. Interaction potentials for alumina and molecular dynamics simulations of amorphous and liquid alumina. J Appl Phys 2008;103:083504.
[22] Siegel DJ, Hector Jr LG, Adams JB. Adhesion, atomic structure, and bonding at the Al(1 1 1)/α-Al_2O_3 (0 0 0 1) interface: a first principles study. Phys Rev B 2002;65:085415.
[23] Lide DR. CRC Handbook of chemistry and physics. 82nd ed. Boca Raton: CRC Press; 2001.
[24] Zheng J-C, Wang H-Q, Wee ATS, Huan CHA. Structural and electronic properties of Al nanowires: an ab initio pseudopotential study. Int J Nanosci 2002;1(2):159–69.
[25] Ghosh PK, Ray S. Effect of porosity and alumina content on the mechanical properties of compocast aluminum alloy–alumina particulate composite. J Mater Sci 1986;21:1667–74.
[26] Ceschini L, Minak G, Morri A, Tarterini F. Forging of the AA6061/23vol.%Al_2O_3 p composite: effects on microstructure and tensile properties. Mater Sci Eng A 2009;513–514:176–84.
[27] Streitz FH, Mintmire JW. Atomic scale simulations of tensile failure in metal oxides. Mater Res Soc Symp Proc 1995;357:459–63.
[28] Zhang W, Smith JR. Nonstoichiometric interfaces and Al_2O_3 adhesion with Al and Ag. Phys Rev Lett 2000;85(15):3225–8.
[29] Rice JR. Elastic fracture mechanics concepts for interfacial cracks. Trans ASME J Appl Mech 1988;55:98–103.
[30] Tvergaard V. Effect of fiber debonding in a whisker-reinforced metal. Mater Sci Eng A 1990;125:203–13.
[31] Kruzic JJ, McNaney JM, Cannon RM, Ritchie RO. Effects of plastic constraint on the cyclic and static fatigue behavior of metal/ceramic layered structures. Mech Mater 2004;36:57–72.
[32] Wang HF. Processing and mechanical properties of interfaces in Al/Al_2O_3 composites. Key Eng Mater 1995;108–110:97–104.
[33] Kim I-S, Lee I. Alumina-composites made by reactive infiltration of molten aluminum alloy into fibrous insulation board. J Mater Sci Lett 1999;18:1945–8.
[34] Iwasa M, Bradt RC. Fracture toughness of single-crystal alumina. Adv Ceram Struct Prop MgO Al_2O_3 Ceram 1983;10:767–79.
[35] Munro RG. Evaluated material properties for a sintered α-Alumina. J Am Ceram Soc 1997;80(8):1919–28.
[36] Buehler MJ, Yao H, Gao H, Ji B. Cracking and adhesion at small scales: atomistic and continuum studies of flaw tolerant nanostructures. Modell Simul Mater Sci Eng 2006;14:799–816.
[37] Prater WL. Comparison of ceramic material effects on the flexural Weibull statistics and fracture of high volume fraction particle reinforced aluminum. Mater Sci Eng A 2006;420:187–98.